Supplementary Material: Real-time examination of atomistic mechanisms during shock-induced structural transformation in silicon

Stefan J. Turneaure, N. Sinclair and Y. M. Gupta

Institute for Shock Physics and Department of Physics, Washington State University,

Pullman, Washington 99164-2816

1. Silicon samples

The nominally pure polycrystalline silicon sample was cut from a 300 mm diameter 3.5 mm thick wafer from JX Nippon Mining & Metals. The polycrystalline sample was fully dense with ρ=2.33 gm/cm^3, determined using the Archimedean method. The relative intensities of the 111, 220, 311, 400 and 311 x-ray diffraction peaks are consistent with a random distribution of the grain orientations; Fig. S1 shows that the integrated diffraction peaks from the diffraction image in Fig. 2a for the polycrystalline Si sample have relative peak intensities that match the relative intensities of simulated cubic diamond Si diffraction peaks (assuming random grain orientation). The average grain size, reported by the vendor, was about 4 μm.
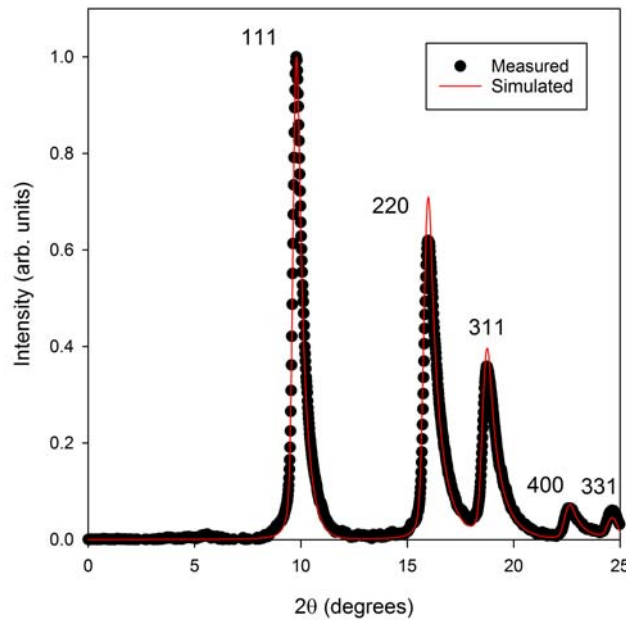

FIG. S1. Measured and simulated diffraction peaks for the ambient polycrystalline silicon sample. The red lines are simulated diffraction peaks assuming randomly oriented cubic diamond silicon grains. The peaks are labeled according to their hkl Miller indices. The integrated diffraction peaks correspond to the XRD pattern in Fig. 2a of the main text.

The Si(100) and Si(111) single crystals were prepared from 0.5 mm thick 25.4

mm diameter undoped silicon wafers from Marketech International. The densities of the

single crystal Si samples were ρ=2.33 gm/cm^3. Laue XRD measurements were used to

verify the nominal orientation of the Si single crystals and to roughly determine the

transverse orientation of the Si single crystals as mounted on the targets. The precise

orientations of the Si single crystals were determined from the Laue spots recorded from

the ambient Si samples mounted on the 2-stage gas gun target holder just prior to the

impact experiments (see Figs. S8a and S9a).

2. Impact experiments and continuum response

Table S1 lists the detailed parameters for each experiment including projectile

velocity, silicon thickness, polycarbonate (PC) window thickness and times relative to

impact at which the x-ray diffraction frames were obtained.

Table S1: Experimental Parameters

Exp. No.	Polycarbonate projectile velocity (m/s)	Si type	Si thickness (mm)	Polycarbonate x-ray window thickness (mm)	Time of 1st frame relative to impact* (ns)
1 (14-5-040)	5170	poly	0.842	1.412	99
2 (14-5-041)	5080	(100)	0.421	1.211	131
3 (14-5-042)	5050	(111)	0.492	1.321	29

*XRD frame times for the 2nd to 4th frames are 153.4 ns, 306.8 ns and 460.2 ns
after the first XRD frame time.

Silicon subjected to plate impact loading with impact stress greater than 16 GPa

develops a transmitted three-wave structure corresponding to an elastic shock, an

inelastic shock and a phase transformation shock wave [1,2]. The Hugoniot elastic limit

3

(HEL) is orientation dependent, but the phase transformation stress is nominally 13-14 GPa and is orientation independent [1,2].

Figure S2 shows a stress-particle velocity diagram for polycarbonate traveling at 5.1 km/s impacting silicon backed by a polycarbonate window. The intersection of the silicon Hugoniot and the polycarbonate impactor Hugoniot indicates an impact stress of about 26 GPa (state 3). Because polycarbonate has lower impedance than the silicon the final stress state will be near 19 GPa (intersection of the PC impactor and PC window Hugoniots) after the sample stress state comes to equilibrium via reflected stress waves propagating through the silicon between the PC impactor and PC window.
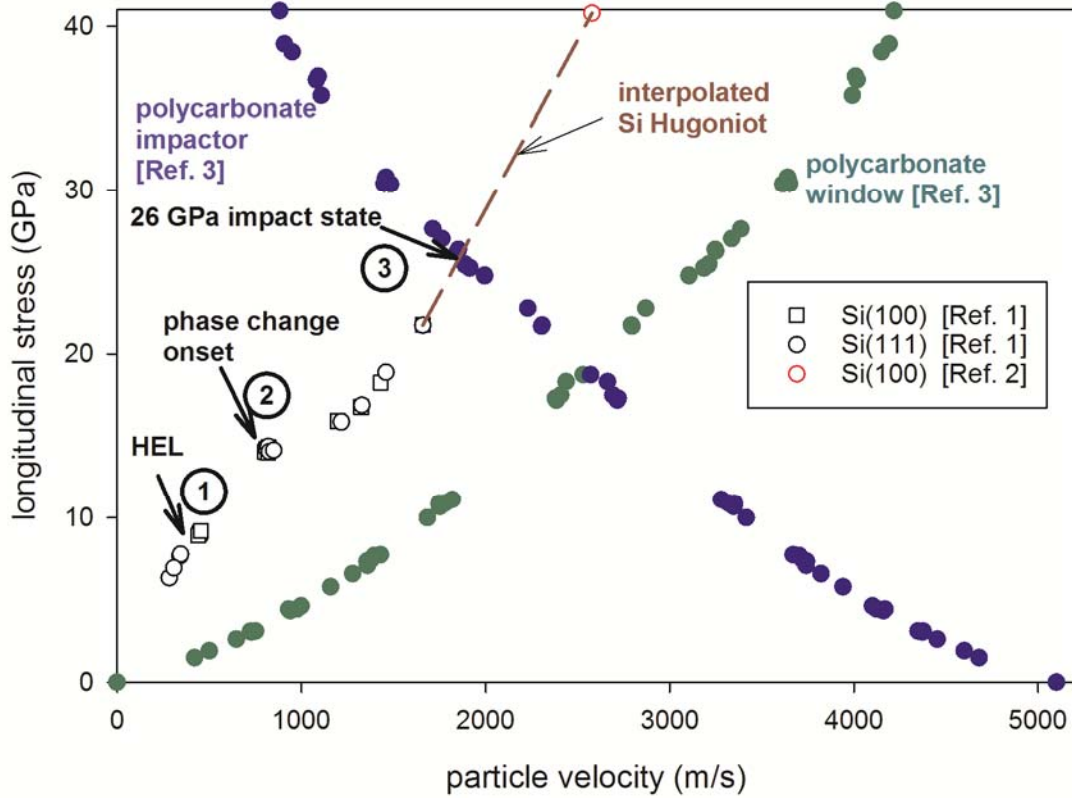

FIG. S2. Stress particle-particle velocity diagram for silicon impact experiments with 5.1 km/s polycarbonate impactor velocity.

Figures S3-S5 show x-t diagrams for the three experiments. After impact, a three-wave shock structure propagates through the Si. The three shock waves bring the material to the HEL (state 1), the phase change threshold (state 2), and the 26 GPa impact stress state (state 3), respectively. As shown in Figs. S3-S5, the first partial stress release (from the elastic shock in the silicon reflecting from the PC window) reaches the incident phase transformation shock after the phase transformation shock wave had propagated through two thirds of the silicon sample thickness. A simple x-t diagram such as shown in Figs. S3-S5 is inadequate to describe the propagation of the phase transformation wave towards the silicon/PC interface after the reflection of the elastic shock from the PC
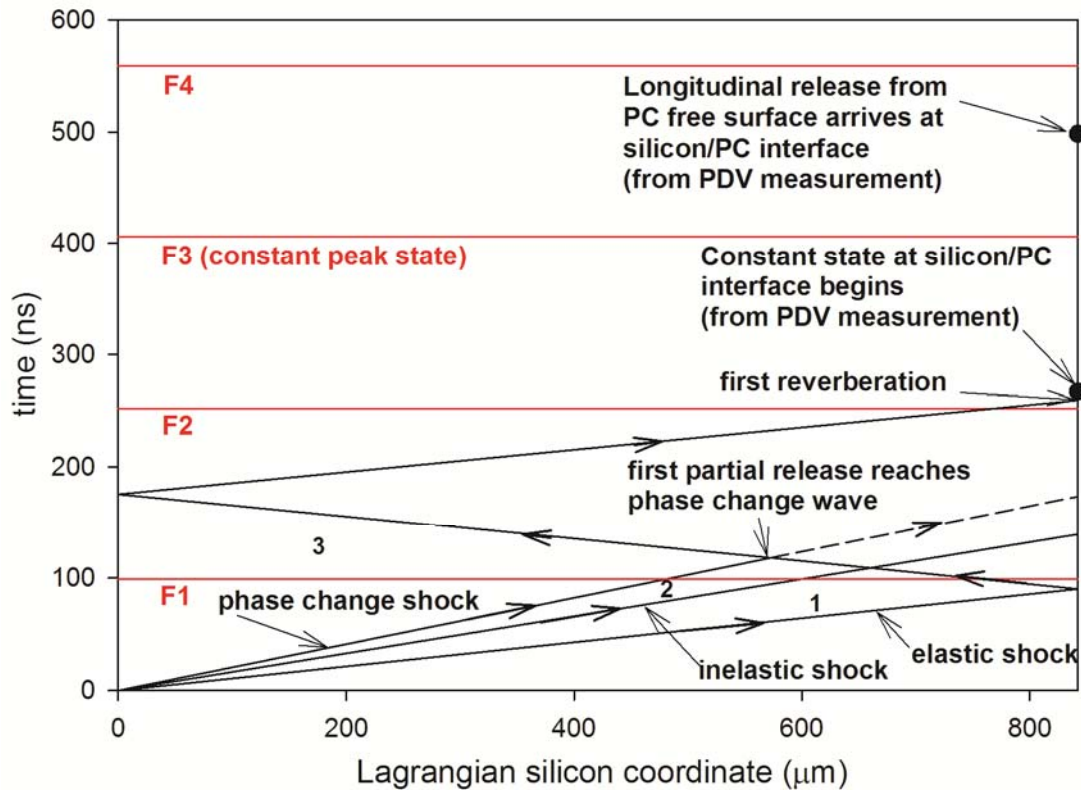

FIG. S3. Position-time diagram for Expt. 1 on shocked polycrystalline Si. The red lines indicate the times relative to impact at which the XRD frames were obtained.
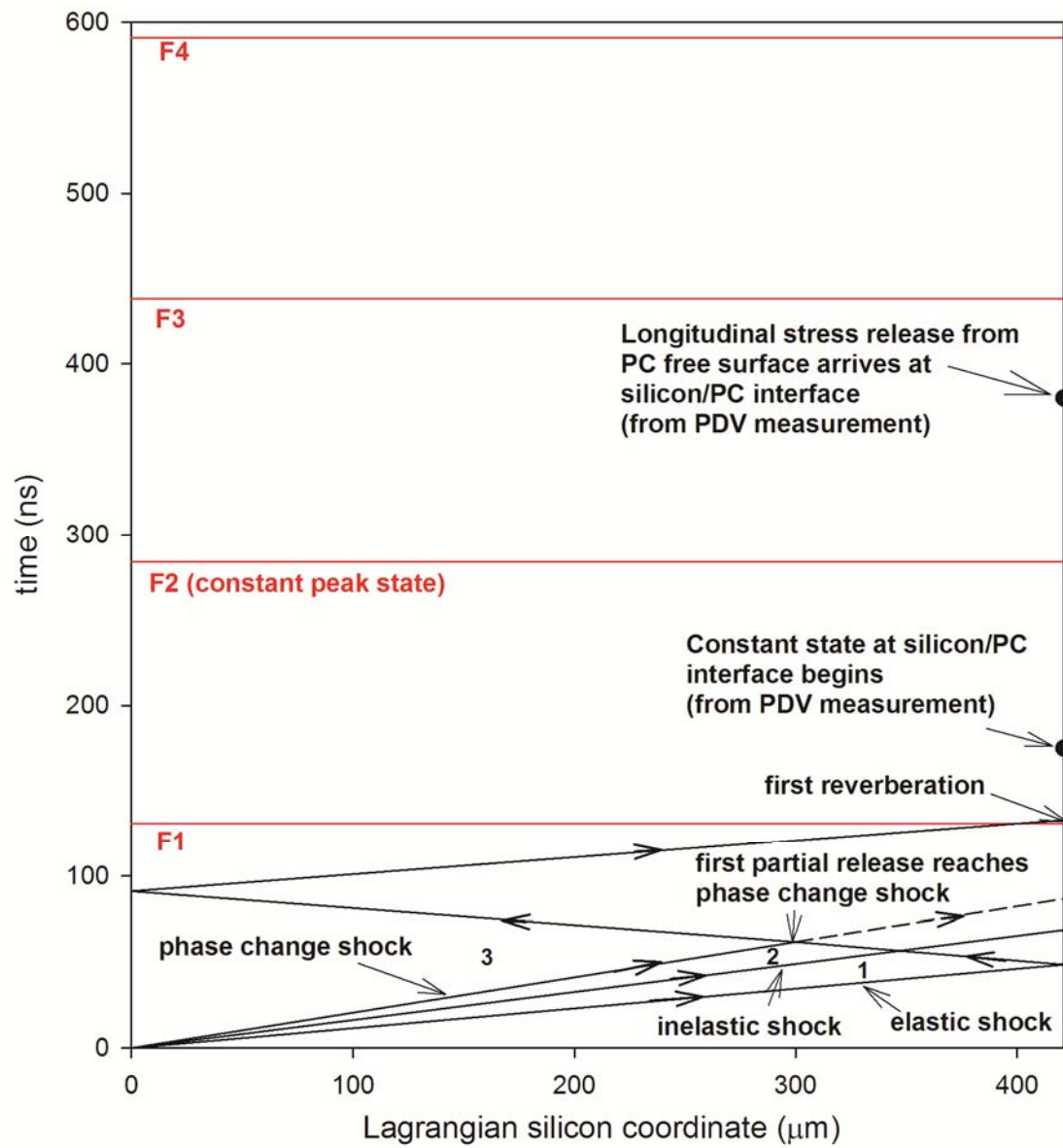
5

FIG. S4. Position-time diagram for Expt. 2 on shocked Si(100). The red lines indicate the times relative to impact at which the XRD frames were obtained.
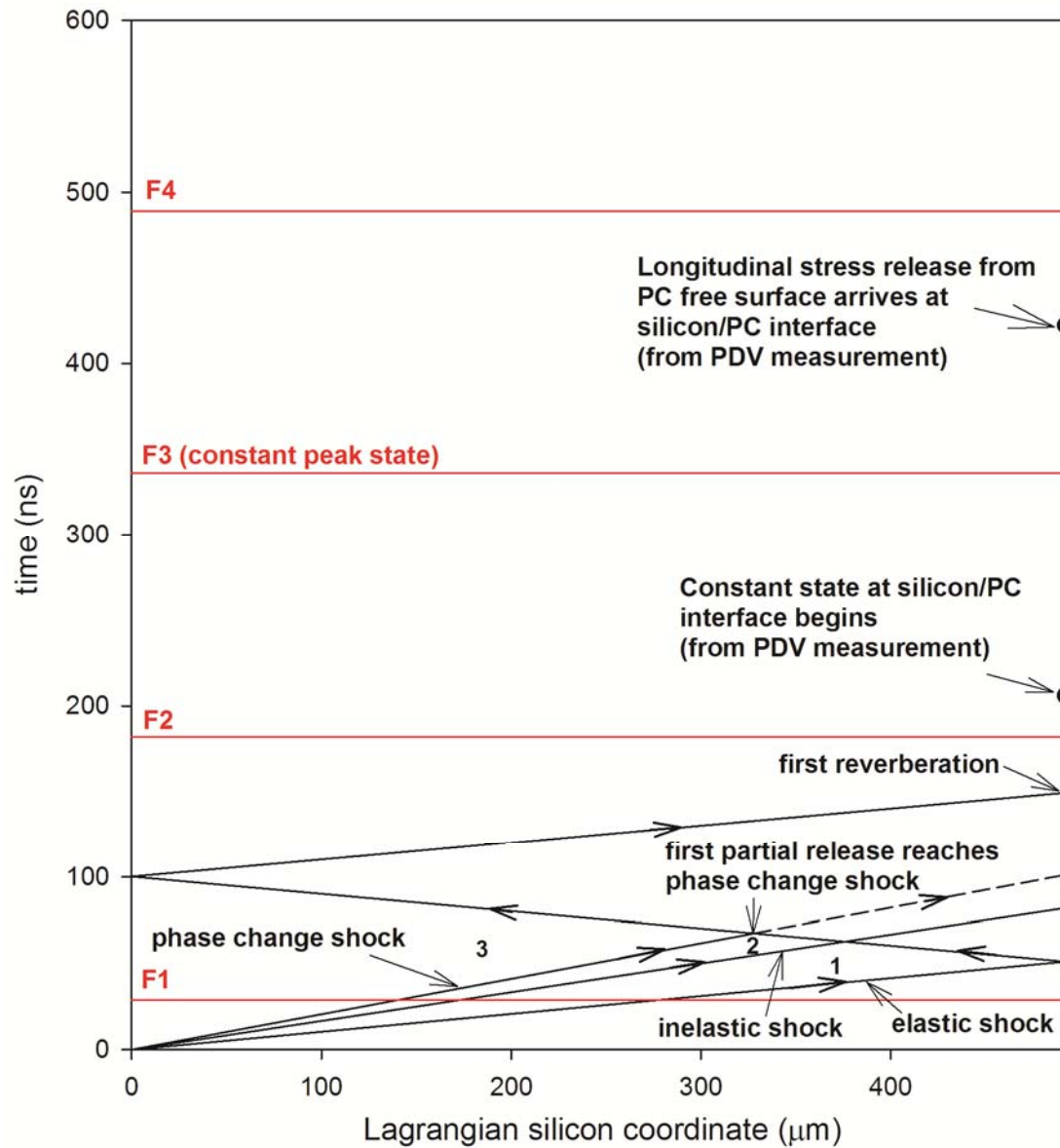
FIG. S5. Position-time diagram for Expt. 3 on shocked Si(111). The red lines indicate the times relative to impact at which the XRD frames were obtained.

window reaches the incident phase transformation wave because of the complex

interactions between the incident 3-wave structure and the waves reflecting from the PC

window; therefore, the continuation of the phase transformation wave towards the

silicon/PC interface after meeting the first partial stress release is approximately indicated by a dashed line in the x-t diagrams. However, from Ref. 1, the material behind the phase transformation shock wave is fully transformed to a high pressure structure and the Lagrangian wave speed in the transformed material is 10.0 km/s. Hence, in Figs. S3-S5, we show the round-trip reverberation of the reflected wave caused by the initial elastic shock reaching the silicon/PC interface. The XRD frames analyzed in detail (labeled as constant peak state in Figs. S3-S5) were obtained after about two round-trip stress wave reverberations through the transformed silicon suggesting a constant stress state has been obtained throughout the silicon thickness.

Photon Doppler velocimetry (PDV) measurements performed at the silicon/PC interface confirm that a constant stress state was obtained in the silicon for XRD frames F3, F2 and F3 for Expts. 1-3, respectively. The particle velocity histories at the silicon/PC interfaces (from the PDV measurements) are shown in Fig. S6 for the three experiments. The first sharp jump in the particle velocity at the silicon/PC interface is due to the elastic shock in the silicon arriving at the interface. Because of the complex wave interactions (in the latter third of the silicon thickness) occurring as the 3-wave structure approaches the silicon/PC interface, the distinct inelastic and phase transformation shock waves observed when using a LiF interferometry window [1] are not observed at the silicon/PC interface; the loading to the constant 19 GPa state is smeared out in time due to wave interactions. As seen in Fig. S6, once the loading to a constant state is complete, the constant state is maintained for about 200 nanoseconds during which an XRD image was obtained. Following the constant state, the silicon/PC interface velocity begins to increase corresponding to the first stress release from the PC

free surface reaching the silicon/PC interface. The times at which the constant states

begin and the times at which the first stress release from the PC free surface reaches the

silicon/PC interface are indicated in the x-t diagrams in Figs. S3-S5 and in Fig. S6.
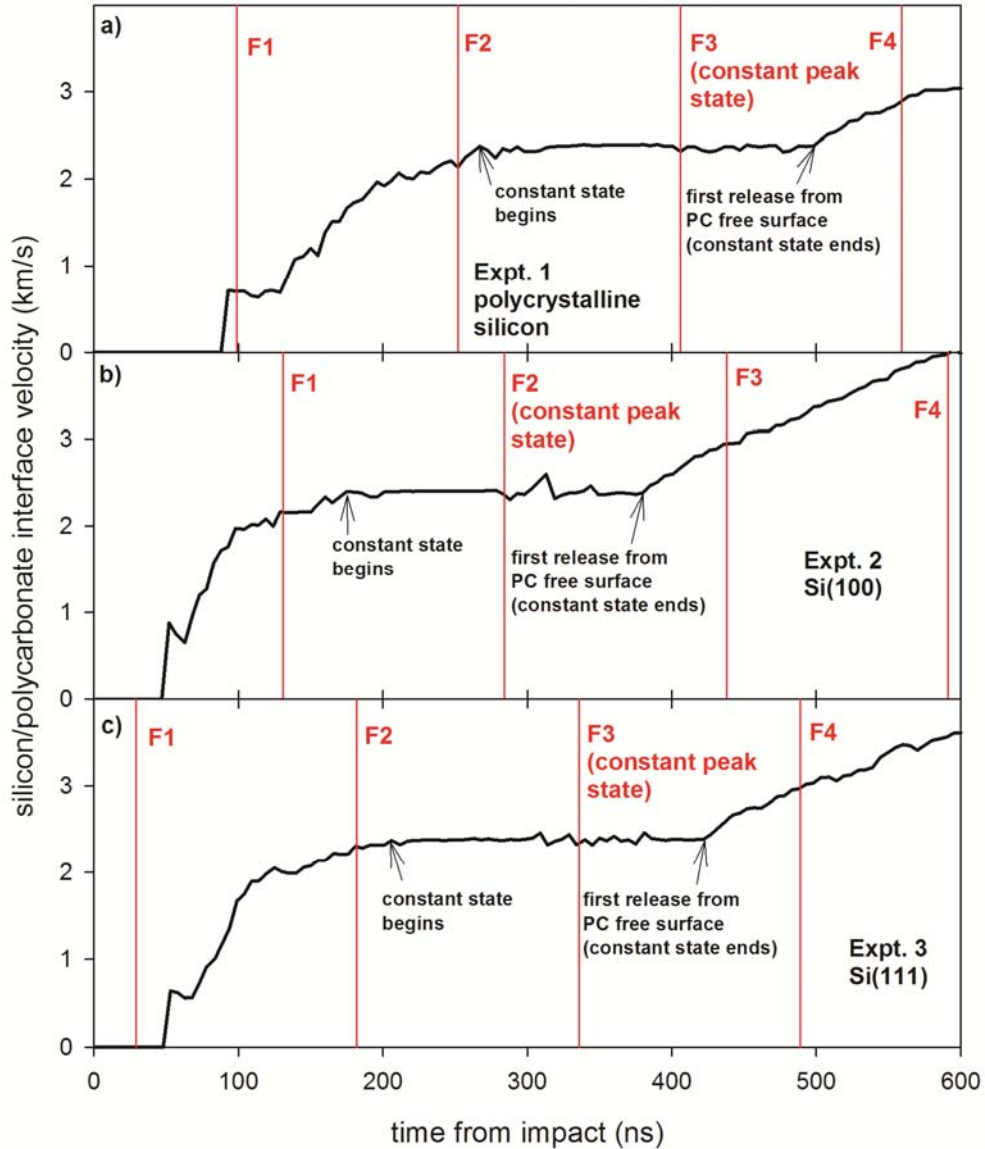

FIG. S6. Particle velocity histories at the silicon/PC window interfaces. The first shock
arriving at the silicon/PC interface is the elastic shock in the silicon. Following the
elastic shock arrival the loading history at the silicon/PC interface is ramped until a
constant state of about 19 GPa is reached. The constant state exists for several hundred
nanoseconds before the particle velocity increases further due to longitudinal stress
release waves arriving from the PC rear free surface.

3. X-ray diffraction measurements

The first harmonic x-rays produced by a 3.6 m long, 1.8 cm period undulator insertion device were used for the x-ray diffraction measurements. A vertical and horizontal KB mirror pair in the 35-ID-A hutch was used to focus the x-rays near the target in the 35-ID-E hutch. The KB mirror filtered out most of the higher harmonic x-rays, but there were sufficient second and/or third harmonic x-rays to observe several weak Laue spots for the ambient single crystal samples (see Figs. S8a and S9a). The focused x-ray beam size passing through the sample was approximately 600 μm horizontally x 800 μm vertically. The x-ray flux spectrum measured using a channel cut monochromator and a diode detector is shown in Fig. S7. The spectral flux was
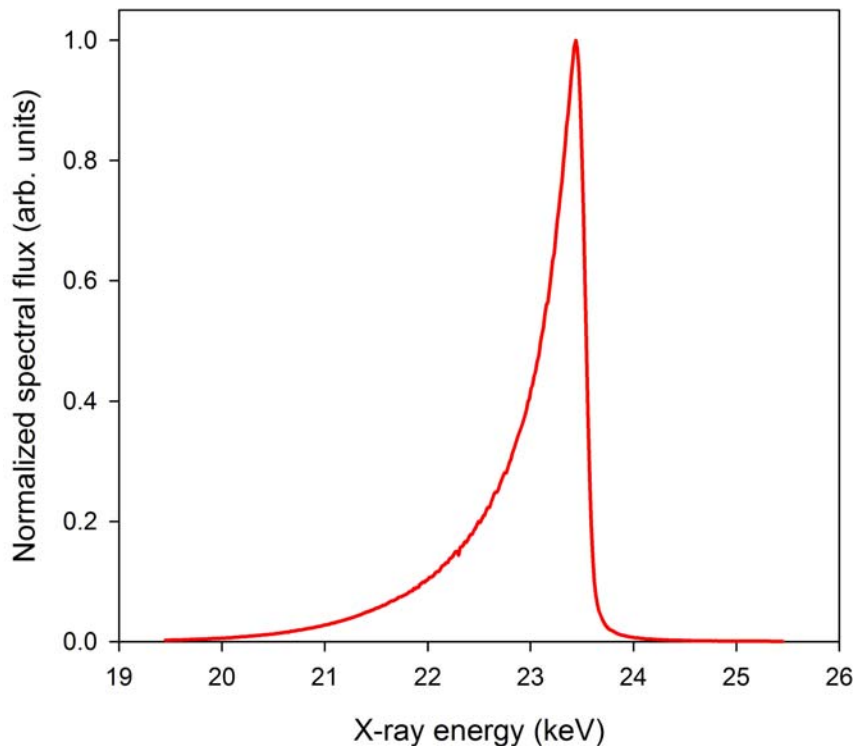

FIG. S7. Measured normalized flux spectrum incident on the 2-stage gas gun target chamber.

maximum at 23.45 keV and the FWHM of the first harmonic was 450 eV with an asymmetric flux spectrum peak shape typical of undulators with a slowly decaying tail at low energies and a sharp drop at energies just above 23.45 keV.

The incident x-ray beam passed into the target chamber through a polycarbonate window; a brass sheet with a small aperture located on the inside wall of the target chamber side flange allowed the direct beam to pass through while blocking much of the scatter produced by the polycarbonate window. A tungsten beamstop was mounted on the target downstream of the sample to stop the direct beam from passing through the downstream target chamber polycarbonate window in front of the x-ray detector; this prevented additional unwanted polycarbonate x-ray scatter from reaching the x-ray detector.

The x-ray detector had a 75 mm diameter active area and was nominally oriented perpendicular to the x-ray beam. The x-ray detector has a front-end which converts the incident x-ray signal to visible light. The detector front-end consists of an Lu_2SiO_5:Ce phosphor screen coated on a radiation hard fiber optic faceplate, a 75:40 mm fiber optic taper and a 40 mm diameter pre-amplifying micro-channel plate image intensifier (II) with P47 phosphor (Sydor Instruments). The output of the II was split using beamsplitters and imaged onto four PI-MAX4:2048f intensified charge-coupled-device (ICCD) detectors (Princeton Instruments). Each ICCD was gated on to detect scattered x-rays from successive synchrotron x-ray bunches (153.4 ns period). The distance from the x-ray beam/sample intersection was about 150 mm from the direct x-ray beam/detector phosphor screen plane intersection. The precise sample to detector distance was determined from measuring XRD patterns from a polycrystalline Si sample

and performing XRD simulations using the flux spectrum shown in Fig. S7 and varying

the sample to detector distance in the simulation until the measured and simulated

diffraction peak positions match as in Fig. S1. The x-ray detector was offset horizontally

such that the direct beam was near the edge of the 75 mm diameter field of view in order

to record diffraction from more hkl planes. The beam/sample intersection on the detector

was determined from XRD patterns from polycrystalline Si and the FIT2D [4,5] silicon

calibrant feature.

4. X-ray diffraction results

Figure 2 in the main text and Figs. S8 and S9 show the complete series of

diffraction images (ambient image and four images obtained during the impact event) for
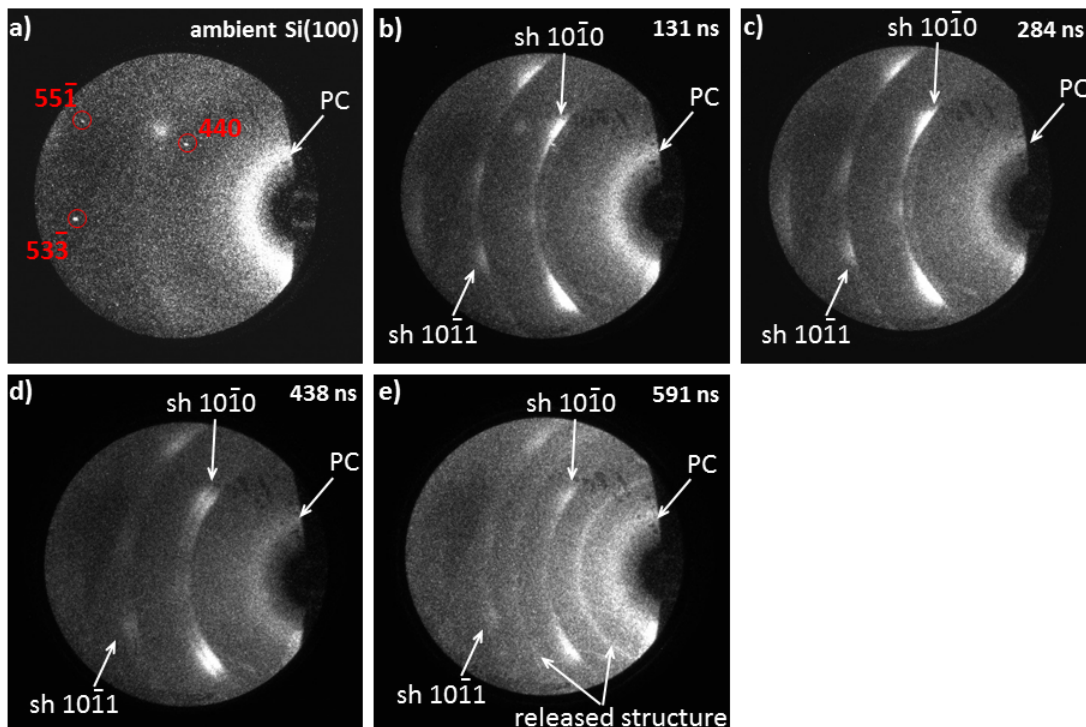

FIG. S8. Full sequence of x-ray diffraction images for the experiment on shocked Si(100). The ambient cd phase Si Laue spots are indexed in (a). The times listed in (b)-(e) are the times at which the diffraction images were taken relative to the impact time. Image (c) best represents the peak shocked state (19 GPa). Images (d) and (e) exhibit features due to stress release.
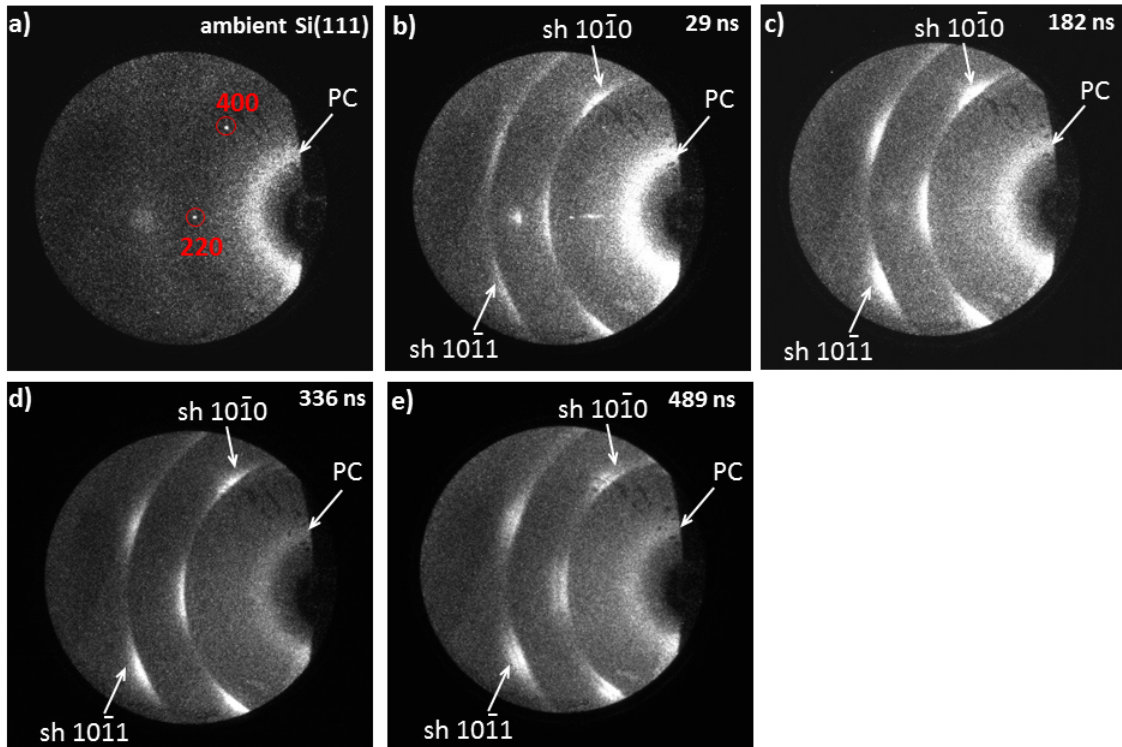
FIG. S9. Full sequence of x-ray diffraction images for the experiment on shocked Si(111). The ambient cd phase Si Laue spots are indexed in (a). The times listed in (b)-(e) are the times at which the diffraction images were taken relative to the impact time. Image (d) best represents the peak shocked state (19 GPa). Image (e) exhibits features due to stress release.

the impact experiments with the polycrystalline Si, Si(100), and Si(111) samples, respectively. For each experiment, one frame was obtained while the silicon was in a constant state of about 19 GPa and the XRD analysis of these frames is discussed in the main text. The other diffraction images not corresponding to a constant peak state can be correlated to the continuum loading history by looking at the x-t diagrams in Figs. S3-S5 and the silicon/PC particle velocity histories shown in Fig. S6. For completeness, some qualitative features of the three other non-constant state images obtained in each impact experiment are described below.

As discussed in the main text, the first frame after impact (99s) for the shocked polycrystalline Si in Expt. 1 (Fig. 2b) corresponds to the phase change shock traveling through half of the Si sample as shown in Fig. S3. As such, in Fig. 2b the diffraction image contains both cd diffraction rings from the latter half of the silicon and sh diffraction rings from the front half of the silicon through which the phase transformation wave has propagated. The diffraction image in Fig. 2c (252 ns) after impact corresponds to a nearly constant state with sh silicon (the very faint 111 and 220 cd peaks are due to an afterglow effect of the detector phosphor). The diffraction image in Fig. 2e (559 ns) corresponds to a time after partial stress release from the unloading at the PC free surface has reached the silicon (see Figs. S3 and S6), but the silicon remains in the sh structure.

For Expt, 2, the image in Fig. S8b corresponds to a nearly constant state with fully transformed silicon and the diffraction pattern is nearly identical to the image in Fig. S8c corresponding to the constant 19 GPa state. The images in Figs. S8d and S8e correspond to times after partial stress release from the PC free surface has reached the silicon sample (see Figs. S4 and S6) and the images exhibit features due to the stress release (doublet simple hexagonal rings in Fig. S8d and appearance of new diffraction rings in Fig. S8e). Edge release waves have reached the volume probed by x-rays by 591 ns after impact so the new diffraction rings appearing in Fig. S8e upon stress release have not been quantitatively analyzed.

For Expt. 3, the image in Fig. S9b (29 ns after impact) corresponds to the phase transformation shock wave having propagated through 30% of the silicon sample and the partial rings observed are from simple hexagonal silicon at 26 GPa behind the phase transformation shock wave. The image in Fig. S9c (182 ns after impact) corresponds to a

nearly constant state with fully transformed silicon and the image in Fig. S9d corresponds to the constant state with about 19 GPa stress. The image in Fig. S9e was obtained after partial stress release from the PC free surface had reached the silicon sample (see Figs. S5 and S6) and the image exhibits doublet simple hexagonal rings due to the partial stress release.

The multi-frame images for the shocked single crystals in Figs. S8 and S9 reveal an important qualitative finding: the localized diffraction spots around the simple hexagonal diffraction rings are independent of whether they are from the initially transformed material at 26 GPa (e.g. Fig. S9b), from material equilibrated at a constant stress state (e.g. Figs. S8c or S9c) or from partially stress released material (e. g. Figs. S8d or S9e). This finding demonstrates that the preferred orientation of the simple hexagonal structure is due to the initial structural transformation and is independent of subsequent stress wave reverberations between the PC window and PC impactor and the associated plastic deformation.

5. Reduction of two-dimensional diffraction data

FIT2D software was used to integrate the two-dimensional diffraction data around the γ angle to get the diffracted intensity vs. 2θ scattering angle [4,5]. Intensity was conserved and no corrections were made due to x-ray polarization or geometrical effects so as to be able to directly compare with the powder diffraction simulations. After the one-dimensional line profiles were obtained using FIT2D, a background line profile – due to coherent x-ray scattering in the polycarbonate and incoherent x-ray scattering throughout the target – was subtracted to obtain the measured diffraction profiles shown in Figs. 2f, 3a, 3d and S1. When converting the measured diffraction peaks from the

silicon samples – recorded after impact had occurred – from radial detector position to 2θ scattering angle, the distance from the sample center to the detector (~150 mm) was adjusted relative to the ambient distance by several hundred micrometers to account for silicon sample compression and translation due to the impact.

6. Powder diffraction simulations

The simulations of diffracted intensity vs. 2θ scattering angle were performed by discretizing the silicon sample into small volume elements and discretizing the calculated incident x-ray spectral flux (see Fig. S7) from the 1st harmonic of the 1.8 cm period undulator by energy. The diffracted intensities from each set of {hkl} planes reaching the detector active area were summed from each discretized volume element and each discretized x-ray energy and binned into discretized 2θ scattering angles. The discretized volume elements had dimensions of approximately 100 μm and the discretized energy spectrum had widths of 13.7 eV. Factors included in the diffracted intensities were the relative incident number of x-rays, the structure factor, the hkl multiplicity factor, the polarization factor, and absorption of the incident and diffracted x-rays by the silicon sample. The calculated diffracted intensities vs. 2θ were convoluted with a 130 μm HWHM Lorentzian to account for instrumental broadening in the detector x-ray phosphor screen. For the simulations of the silicon samples in the shocked state, the distance from the sample center to the detector (~150 mm) was adjusted relative to the ambient distance by several hundred micrometers to account for silicon sample compression and translation due to the impact.

7. Diffraction simulations for textured simple hexagonal silicon

The ambient cd orientations were roughly known from the nominal crystal orientations and determined precisely from the measured Laue spots from the crystal prior to impact. For a given diffraction simulation, a particular set of orientation relations (ORs) between the ambient cd structure and the shocked sh structure was assumed; in general for any given type of OR, the sh structure has multiple orientations (N_{sh}) that are equivalent by symmetry to the ambient cd structure. In the simulations, it was assumed that each of the degenerate N_{sh} orientations occurs with equal probability and that for each of the sh structure orientations there is a distribution of orientations about the nominal sh structure orientation to account for the finite breadth of the observed diffraction spots in the azimuthal direction (γ angle); the orientation distribution was chosen to be uniform for rotations up to 10 degrees from nominal and to decrease as the inverse squared of the misorientation angle for misorientations larger than 10 degrees. In the simulations, only diffraction from sh lattice planes that can have diffracted intensity on the detector from the undulator 1st harmonic were considered. A large number of random samples were taken for the distributed orientations of the N_{sh} degenerate nominal orientations. For each random sh orientation, the wavelength required to satisfy the Laue condition was calculated. If the required wavelength was within the 1st harmonic of the incident spectral flux, the pixel where the outgoing wavevector intersected with the detector was calculated and additional diffracted intensity was assigned to that pixel. The additional diffracted intensity was proportional to the spectral flux at the wavelength satisfying the Laue diffraction condition and also proportional to the structure factor of the particular diffraction peak.

Supplementary Figs. S10 and S11 show the measured diffraction patterns in the peak shocked state for the experiments on Si(100) and Si(111) samples, respectively. Also shown are the diffraction simulations for 12 different sets of ORs (see Table S2) relating the orientations of cd and sh silicon. OR set #5 was the one used for Fig. 3 in the main text. Note that for the Si(111) experiment, simulations using OR sets #1, #3 and #12 in Fig. S5 look qualitatively similar to the measured diffraction pattern, but in all three simulations the centrally located diffraction peak is from $\{0001\}$ type simple hexagonal planes, whereas in the experiment, the centrally located diffraction peak is from a $\{10\bar{1}0\}$ type sh plane.

Table S2: List of trial orientation relation (OR) sets between cubic diamond (cd) and simple hexagonal (sh) silicon structures

OR set #	Relation A*	Relation B*	N_{sh}^
1	$<110>_{cd}//<0001>_{sh}$	$<1\bar{1}1>_{cd}//<10\bar{1}0>_{sh}$	12
2	$<110>_{cd}//<0001>_{sh}$	$<1\bar{1}0>_{cd}//<10\bar{1}0>_{sh}$	6
3	$<110>_{cd}//<0001>_{sh}$	$<001>_{cd}//<10\bar{1}0>_{sh}$	6
4	$<110>_{cd}//<0001>_{sh}$	$<1\bar{1}1>_{cd}//<11\bar{2}0>_{sh}$	12
5	$<111>_{cd}//<0001>_{sh}$	$<10\bar{1}>_{cd}//<10\bar{1}0>_{sh}$	4
6	$<111>_{cd}//<0001>_{sh}$	$<10\bar{1}>_{cd}//<11\bar{2}0>_{sh}$	4
7	$<100>_{cd}//<0001>_{sh}$	$<001>_{cd}//<10\bar{1}0>_{sh}$	6
8	$<100>_{cd}//<0001>_{sh}$	$<011>_{cd}//<10\bar{1}0>_{sh}$	6
9	$<211>_{cd}//<0001>_{sh}$	$<1\bar{1}\bar{1}>_{cd}//<10\bar{1}0>_{sh}$	12
10	$<211>_{cd}//<0001>_{sh}$	$<1\bar{1}\bar{1}>_{cd}//<11\bar{2}0>_{sh}$	12
11	$<110>_{cd}//<0001>_{sh}$	$<1\bar{1}2>_{cd}//<10\bar{1}0>_{sh}$	12
12	$<110>_{cd}//<0001>_{sh}$	$<1\bar{1}2>_{cd}//<11\bar{2}0>_{sh}$	12

*Each OR set is composed of two relations of parallel cd and sh crystallographic directions labeled Relation A and Relation B.
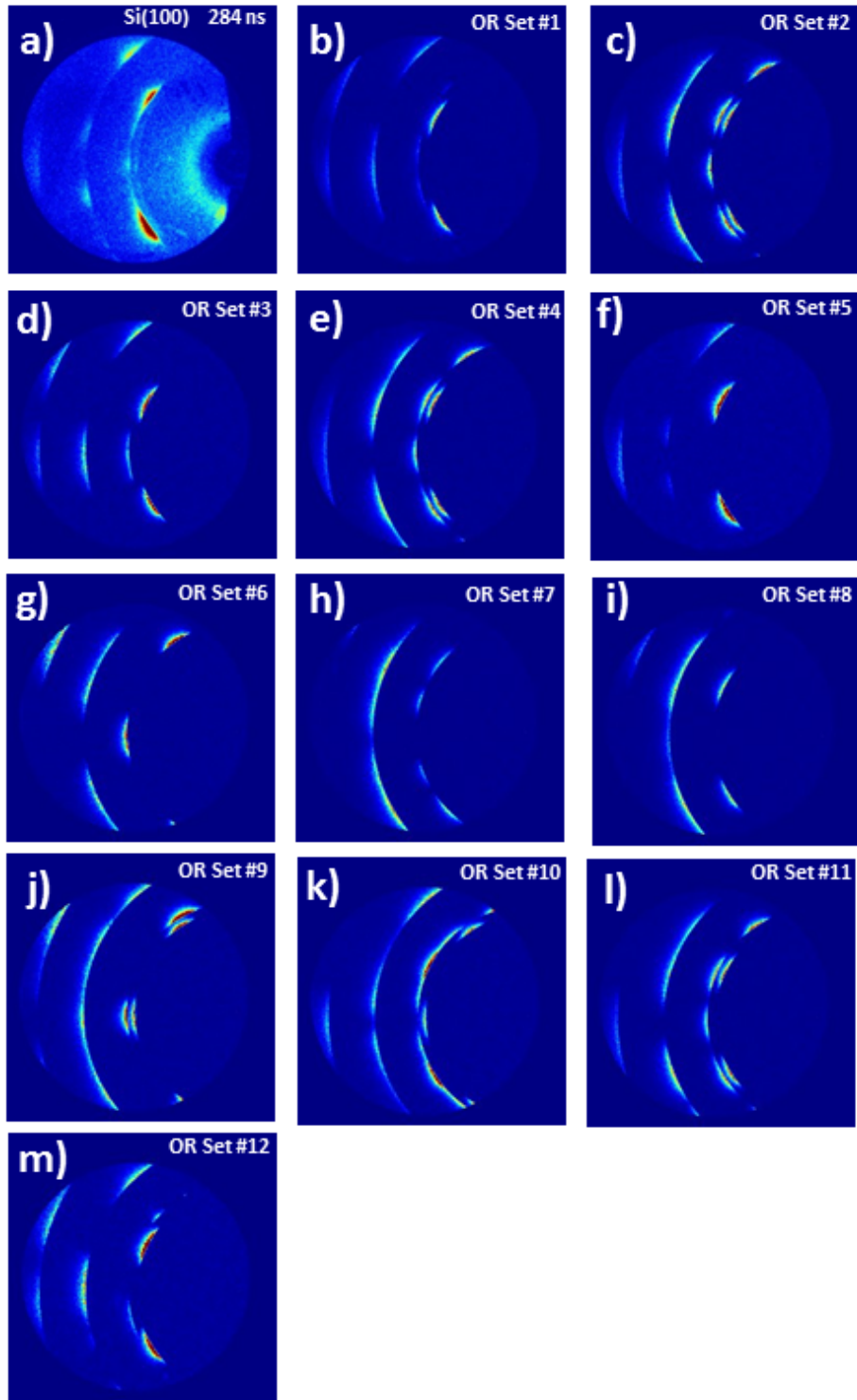^N_{sh} is the degeneracy of a given orientation relation set.

FIG. S10. Measured and simulated peak state (19 GPa) x-ray diffraction images for Si shocked along [100]. (a) Measured peak state diffraction pattern 284 ns after impact. (b)-(m) Simulated diffraction patterns using orientation relation (OR) sets listed in Table S2. The simulation using OR Set#5 in (f) best matches the measured diffraction pattern.
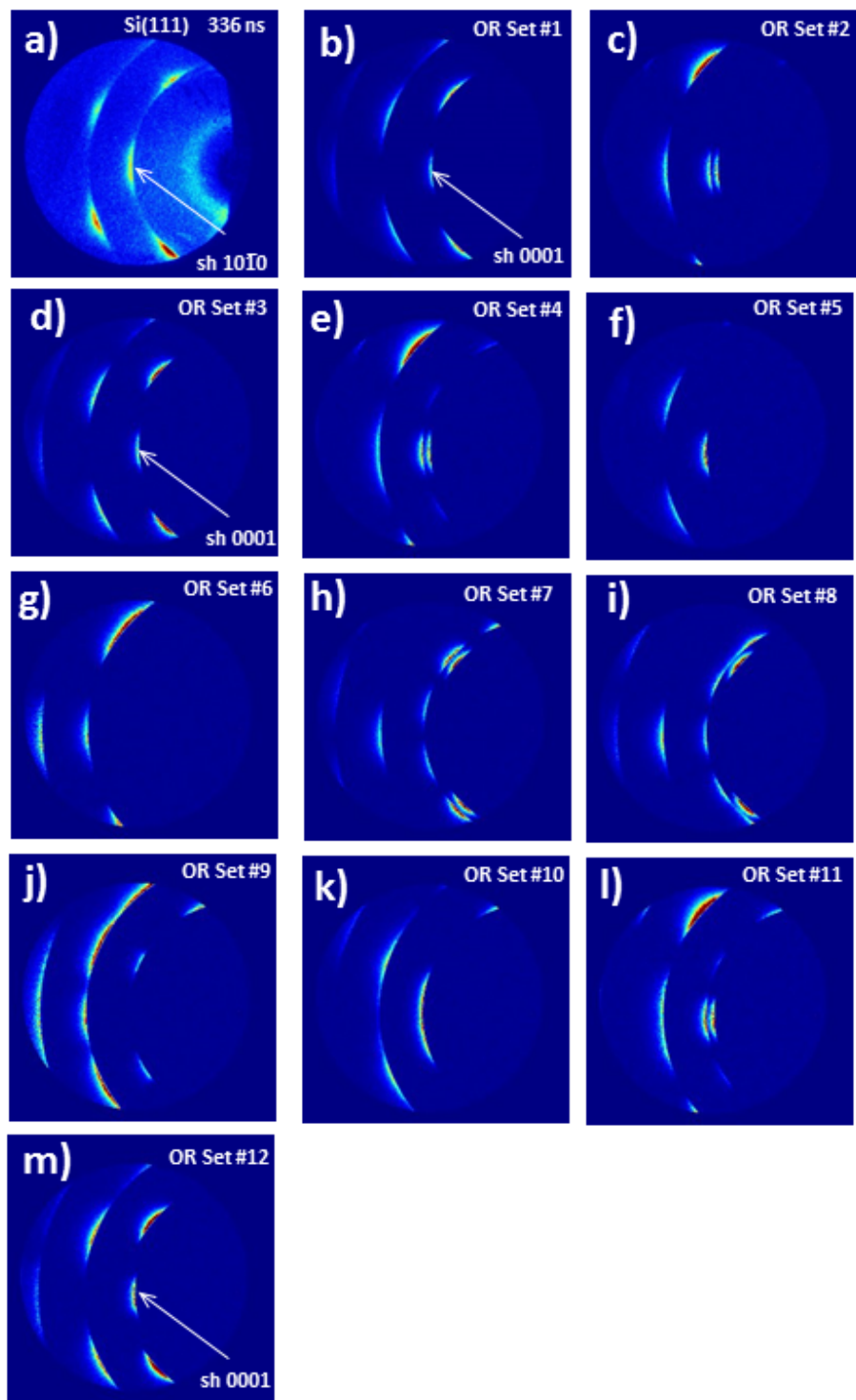
FIG. S11. Measured and simulated peak state (19 GPa) x-ray diffraction images for Si shocked along [111]. (a) Measured peak state diffraction pattern 336 ns after impact. (b)-(m) Simulated diffraction patterns using orientation relation (OR) sets listed in Table S2. The simulation using OR Set#5 in (f) best matches the measured diffraction pattern.

List of References

1. S. J. Turneaure and Y. M. Gupta, Appl. Phys. Lett. **91**, 201913 (2007).

2. T. Goto, T. Sato and Y. Syono, Jpn. J. Appl. Phys. **21**, L369 (1982).

3. S. P. Marsh, LASL Shock Hugoniot Data (University of California, Berkeley, 1980).

4. A. P. Hammersley, FIT2D: An introduction and overview. ESRF Internal Report, **ESRF97HA02T** (1997).

5. A. P. Hammersley, S. O. Svensson, M. Hanfland, A. N. Fitch, D. Hausermann, High Pressure Res. **14**, 235 (1996).